Atmos. Chem. Phys. Discuss., 8, 2275–2309, 2008
www.atmos-chem-phys-discuss.net/8/2275/2008/

Atmospheric Chemistry and Physics Discussions

Characteristics of the NO-NO_2-O_3 system in different chemical regimes during the MIRAGE-Mex field campaign

Z.-H. Shon[1], S. Madronich[2], S.-K. Song[3], F. M. Flocke[2], D. J. Knapp[2], R. S. Anderson[2], R. E. Shetter[2], C. A. Cantrell[2], and S. R. Hall[2]

[1]Department of Environmental Engineering, Dong-Eui University, 995 Eomgwangno, Busan 614-714, Republic of Korea
[2]Atmospheric Chemistry Division, National Center for Atmospheric Research, P.O. Box 3000 Boulder, CO 80307, USA
[3]School of Earth and Atmospheric Sciences, Georgia Institute of Technology, Atlanta, GA 30318, USA

Received: 20 December 2007 – Accepted: 3 January 2008 – Published: 6 February 2008

Correspondence to: Z.-H. Shon (zangho@deu.ac.kr)

Published by Copernicus Publications on behalf of the European Geosciences Union.

Abstract

The NO-NO_2 system was analyzed in different chemical regimes/air masses based on observations of reactive nitrogen species and peroxy radicals made during the intensive field campaign MIRAGE-Mex (4 to 29 March 2006). In general, NO_2/NO ratios, which can be used as an indicator to test current understanding of tropospheric chemistry mechanism, are near photostationary state. The air masses were categorized into 5 groups: boundary layer (labeled as "BL"), free troposphere (continental, "FTCO" and marine, "FTMA"), biomass burning ("BB"), and Tula industrial complex ("TIC"). The time- and air mass-dependent NO_2/NO ratios ranged from 2.35 (TIC) to 5.18 (BB), while the NO_x/NO_y ratios varied from 0.17 (FTCO) to 0.54 (BL). The ozone production efficiency for the 5 air mass categories ranged from 5.0 (TIC) to 10.2 (BL), indicating photochemically young and reactive air masses.

1 Introduction

During March of 2006, the Megacities Impact on Regional and Global Environment: Mexico (MIRAGE-Mex) field campaign took place in the region of the Mexico City Metropolitan Area (MCMA) including the Gulf of Mexico. This field campaign was designed to examine the chemical and physical transformations of gases and aerosols in the polluted outflow from MCMA and to assess the current and future impacts of these exported pollutants on regional and global air quality, ecosystems, and climate. MCMA is a megacity of about 20 million people residing in an area of 1500 km^2, surrounded by mountains and at an elevation of 2.2 km above sea level (asl). The air quality in MCMA is affected by strong anthropogenic sources of NO_x ($NO+NO_2$) and volatile organic compounds (VOCs) in conjunction with high solar irradiance facilitating photochemistry (Raga et al., 2001). In the 1990's, hourly averaged ozone concentrations in MCMA exceeded the Mexican national standard of 110 ppbv for much of the year (Raga and Raga, 2000).

ACPD

8, 2275–2309, 2008

As essential ingredients for the formation of O_3, the reactive nitrogen species (NO_x) are emitted to the atmosphere mainly in the form of NO from road traffic (Soltic and Weilenmann, 2003). NO and NO_2 are interconverted rapidly through following reactions:

$$NO + O_3 \rightarrow NO_2 + O_2 \tag{R1}$$

$$NO_2 + h\nu(\lambda < 420\,\text{nm})(+O_2) \rightarrow NO + O_3 \tag{R2}$$

$$NO + HO_2 \rightarrow NO_2 + OH \tag{R3}$$

$$NO + RO_2 \rightarrow NO_2 + RO \tag{R4}$$

where RO_2 is any organic peroxy radical including CH_3O_2, and RO is the corresponding alkoxy radical. The NO_2/NO ratio can be formulated as:

$$\frac{[NO_2]}{[NO]} = \frac{(k_1[O_3] + k_3[HO_2] + k_4[RO_2])}{J_2} \tag{1}$$

where k_1, k_3, and k_4 are reaction rate constants for the reactions R1, R3, and R4, respectively and J_2 photolysis frequency of NO_2. Previous studies investigating the NO-NO_2 cyclic system were conducted in urban and remote areas utilizing observations of O_3 (R1) and/or peroxy radicals (R3–R4) (Cantrell et al., 1997; Crawford et al., 1996 and references therein). They found that model-predicted peroxy radicals were often less than those required to explain the observed NO_2/NO ratio. In addition, the model-predicted NO_2 levels were reported to be somewhat lower than observations. For example, comparison between observations and predictions ($[NO_2]_{obs}/[NO_2]_{calc}$) in several field campaigns (CITE-3, ABLE-3B, CITE-2, and TRACE-A) typically showed 1.3 to 1.6 with a maximum of up to 3.4 in PEM-West A (Crawford et al., 1996). In contrast, Ridley et al. (1992) found good agreement between model peroxy radicals and those estimated from the NO_2/NO ratio. Meanwhile, the potential role of iodine chemistry in NO_2/NO ratio change as well as HO_2/OH has been suggested based on field,

ACPD

8, 2275–2309, 2008

model, and kinetic studies (Chameides and Davis, 1980; Davis et al., 1996; Knight and Crowley, 2001; Kanaya et al., 2002, 2007). Since both hydroperoxyl and organic peroxy radicals were measured during the MIRAGE-Mex campaign, the photostationary state (PSS) of the NO-NO_2 system can be assessed based on field observations in this study without model estimates.

To assess the impact of MCMA emission on O_3 and its precursors on regional and hemispheric scales, it is important to evaluate the loss and transformation processes of reactive nitrogen species (NO_x to NO_y, which is total reactive nitrogen oxides) in the course of transport of urban or industrial plumes. The emitted NO_x can be oxidized in the atmosphere by OH, forming HNO_3 which is subject to removal from the air mass through dry and wet deposition. The average lifetime of NO_y in an urban, industrial (Nunnermacker et al., 2000) or continental outflow plumes (Takegawa et al., 2004) ranges from 0.25 to 2 days; whereas that of NO_x in each environment is slightly shorter (less than 0.25 day in the former environment with longer lifetime in the latter environment, e.g., 1.2 days).

High levels of NO_x in the urban plume result from enhanced local emission sources including transportation. Thus, NO_x can be a measure of anthropogenic impacts at the sampling position and the ratio of NO_x to NO_y can be of value in understanding the chemical evolution process as an indicator for photochemical age (Carroll et al., 1992). In this study, we analyzed the NO-NO_2 cyclic system in different chemical regimes/air masses based on observations of reactive nitrogen species and peroxy radicals. The analysis of PSS allows us to assess the current understanding of tropospheric NO_x chemistry including the potential for yet-unidentified chemical reaction. We also examined the NO_x/NO_y ratios and ozone production efficiencies of the polluted outflow from MCMA, providing some insight on the photochemical aging processes in various chemical regimes.

2 Observational data

The intensive field campaign of MIRAGE-Mex was carried out from 4 March to 29 March, involving the NSF/NCAR C-130 aircraft, ground-based measurements, and satellite observations. This campaign made numerous physico-chemical measurements such as reactive nitrogen species, oxidized sulfur species, oxygenated VOCs, aerosols, peroxy radicals, and so on. It also included the measurements of actinic flux and atmospheric photolysis frequencies such as $J(O_3)$, $J(NO_2)$, $J(HNO_2)$, etc. (Shetter et al., 2002). In this study, we focused on the data of chemical measurements of reactive nitrogen species (NO, NO_2, HNO_3, PANs, organic nitrates, particulate nitrate, NO_y) and other trace gases such as O_3, which were made on the C-130. Reactive nitrogen species, including NO, NO_2, NO_y, and O_3 were measured at 1 Hz with a chemiluminescence technique (Weinheimer et al., 1998). HNO_3 and organic nitrates were measured with a chemical ionization mass spectrometer (CIMS, Crounse et al., 2006 and references therein), while PANs were measured with a thermal dissociation CIMS (Slusher et al., 2004). As one of key measurements for the analysis of NO-NO_2 PSS (Eq. 1), peroxy radicals (HO_2+RO_2) were measured with the four-channel CIMS (Cantrell et al., 2003).

Twelve C-130 missions were flown during the campaign, covering the altitude from the surface to about 7 km. Most of the flights sampled air over the MCMA basin and central Mexico, and several of the flights extended over the Gulf of Mexico to sample continental outflow from the MCMA. Table 1 shows detailed information on the 12 flights including spatial and temporal coverage. The data of flight 6 was excluded in the PSS analysis due to malfunction of the ozone instrument. More detailed flight tracks are available at the web site http://www.eol.ucar.edu/flight_data/mirage1/.

ACPD

8, 2275–2309, 2008

3 Results and discussion

3.1 Air mass category and photostationary state analysis of NO-NO_2 system

In order to analyze the NO-NO_2 cycling in different chemical regimes, the air masses were categorized into 5 groups: boundary layer (BL), free troposphere (continental, FTCO and marine, FTMA), biomass burning (BB), and Tula Industrial Complex (TIC). The air mass characterization was determined based on geographical location, meteorological parameters (temperature and relative humidity, etc.), model (Weather Research and Forecasting with Chemistry, WRF-Chem, Tie et al., 2007 and references therein), and observations of trace gases. For instance, the category for the BL air masses was determined based on meteorological parameters and WRF-Chem and those for FTCO and FTMA were based on geographical locations of airborne sampling. In addition, that for the BB was determined based on hydrogen cyanide (HCN), perchlorethene (C_2Cl_4), and CO (Gregory et al., 1996; Li et al., 2000), while that for TIC was based on the concentration levels of CO, NO_x, and SO_2. The average concentrations of HCN, C_2Cl_4, and CO in the BB air masses corresponding to the flights on 4, 22, and 23 March were 965±761 pptv (median of 905), 4.2±7.5 pptv (0.92), and 278±184 ppbv (225), respectively. The median concentration of HCN for the BB is factors of 1.6 (TIC), 1.9 (BL), 2.5 (FTMA), and 2.8 (FTCO) higher than those for other air mass categories. The mean concentrations of SO_2, CO, and NO_x for the TIC corresponding to the data measured on 10, 19, and 22 March were 22±40 (median of 9.4), 186±81 (192), and 2.6±4.4 (0.82) ppbv, respectively. The mean concentration of SO_2 for TIC is higher than those for other air mass categories by factors ranging from 4.7 to 15.

The PSS of NO-NO_2 systems with different air mass categories was analyzed in Fig. 1. The PSS parameter (ϕ) is defined as follows:

$$\phi = \frac{\{k_1[O_3] + k_3[HO_2] + k_4[RO_2]\}/J(NO_2)}{[NO_2]/[NO]} \tag{2}$$

ACPD

8, 2275–2309, 2008

Characteristics of the NO-NO_2-O_3 system during the MIRAGE-Mex

Z.-H. Shon et al.

In Eq. (2), the reaction rate constants (k_1, k_3, and k_4) are taken from Sander et al. (2002) and k_4 is the coefficient corresponding to the reaction between NO with CH_3O_2. If Reactions 1–4 represent adequately the NO-NO_2 partitioning, the value of ϕ (and the slope of Fig. 1) would be expected to be near unity. The PSS parameter (ϕ) ranged from 0.89 (FTMA) to 2.60 (BB) with the slope value of 1.13 for all data (Fig. 1a). The uncertainty (1σ) of the parameter is estimated to range from 23 (BL, FTCO, FTMA, and TIC) to 25% (BB) based on error propagation analysis using measurement uncertainties. In general, NO_2/NO ratios are near PSS, showing a strong correlation (r^2=0.73) with the value of $k_1[O_3]+k_3[HO_2]+k_4[RO_2]\}/J(NO_2)$. The discrepancy between the observed $[NO_2]/[NO]$ ratios (denominator in Eq. 2) and calculated ratios (numerator in Eq. 2) was not always statistically significant for BL, FTMA, and FTCO. In contrast, there was slight deviation from the PSS for TIC. However, there was large deviation from the PSS for the BB air mass and the NO_2/NO ratio in BB (5.18) was higher than those (2.35–4.17) in other air masses. The large deviation from the PSS for the BB might result from significantly less photochemical aging process (or relatively fresh plume), supported by lower ozone production efficiency (OPE of 4.6, detailed discussion in Sect. 3.3) and higher NO_x/NO_y ratio (e.g., 0.3), compared to other air masses. More discussion on the ratio is given below. The discrepancy between the observed and calculated ratios can suggest the possibility of lack of current understanding of the tropospheric chemistry mechanism. The potential role of iodine chemistry in NO_2/NO ratio change has been suggested based on field, model, and kinetic studies (Chameides and Davis, 1980; Davis et al., 1996; Knight and Crowley, 2001). Recently, significant impact of iodine chemistry (e.g., reaction of IO with NO producing NO_2) on the observed NO_2/NO ratio has been reported for the field study at Rishiri island, Japan (Kanaya et al., 2002, 2007). The IO mixing ratio required to reproduce the PSS of NO-NO_2 system were estimated to be 0.8 pptv for FTMA on average. Similar ranges of IO levels (e.g., 0.3 at Cape Grim and 0.5–7 pptv at Mace Head) have been observed in the marine atmosphere (McFiggans, et al., 2000; Allan et al., 2000; Saiz-Lopez and Plane, 2004) and this suggests the potential role of halogen chemistry in NO_2/NO ratio shift.

For the BB, O_3 and NO_x concentrations were relatively higher with mean levels of 74 and 3.1 ppbv, respectively, higher than those for TIC, but less than those for the BL (79 and 3.7 ppbv, respectively) (Table 2). Mean concentrations of NO and NO_2 for the BB were 0.51 and 2.5 ppbv respectively. The mean NO_2 level for the BB was higher than those in other air mass categories by at least a factor of 1.3 and as much as a factor of 11 for the FTCO. The only exception to this was the BL. The relatively high NO_x levels for the BB are likely to be affected by outflow from MCMA. NO_x enrichment was also reported in the forest fire emissions near MCMA during the MIRAGE-Mex campaign on a different airborne platform (Twin Otter), ascribed to the deposition of nitrogen-containing pollutants in the outflow from the MC urban area (Yokelson et al., 2007). The concentrations of peroxy radicals, HO_2 and RO_2 for the BB were 58 and 159 pptv, respectively, which were factors of 1.3 to 4.7 (except for the BL) and 1.6 to 7.2 higher than those in other air mass categories, respectively.

It appears that there is no distinct trend in the PSS parameter ϕ in terms of altitude (above ground level and asl) (Fig. 2). In general, there was large variation in values of the parameter (ϕ) at altitude less than 3 km, as well as around 5 km for FTCO (Fig. 2d). For FTCO, the mixing ratios of air pollutants such as O_3 and NO_x were low in comparison to other air mass categories, with mean values of 51 and 0.3 ppbv. With increasing altitudes, the proportion of ϕ values less than 1 increases, possibly due to the increase of NO_2/NO and/or the decrease of peroxy radical mixing ratios. Overall, there was no distinct PSS dependence on altitude.

According to a previous study of the PSS analysis of NO-NO_2 system (Crawford et al., 1996), the inverse value of the PSS parameter (ϕ^{-1}) was reported to range from 1.33 to 3.36, estimated for several airborne sampling campaigns such as PEM-West A, CITE-3, ABLE-3B, CITE-2, and TRACE-A. From these campaigns, most ϕ^{-1}values were close to 1.4, but that for PEM-West A (3.36) was significantly higher in comparison. The cause for the significantly large deviation from the PSS in PEM-West A was suggested to be interference in the NO_2 measurement and this possibility stimulated improvements to the measurement technique during PEM-Tropics A (Bradshaw et al., 1999). Note that the number of data used in our PSS analysis was somewhat reduced due to lack of peroxy radical observations during the measurement period, compared to the NO_2/NO and NO_x/NO_y data.

3.2 NO_x partitioning for air mass category and photochemical aging

The NO_2/NO ratios for each air mass ranged from 2.35 (TIC) to 5.18 (BB), as shown in Fig. 3. There is significant correlation (r^2=0.55 to 0.88) between NO_2 and NO in each air mass, indicating the same source in each air mass, supported by air mass back trajectory analysis (NOAA HYSPLIT model) (Fig. 4). Figure 4 shows only the most frequent air mass back trajectory for each air mass category. For the BL, westerly winds (W and SW) were predominant (75%) and southwesterly wind (75%) for the BB. For the FTCO, westerly wind was dominant (35%) and southwesterly (41 and 67%) for the FTMA and TIC, respectively. The strong correlation (0.76–0.88) between NO_2 and NO was observed for the BL, BB, FTCO, and TIC air mass, whereas the FTMA category showed relatively weaker correlation (0.55). For the BL air mass, there was slight reduction in correlation intensity due to data on 26 and 29 March (data group in right-hand side (RHS) of curve fit, as shown in Fig. 3a). The re-calculated NO_2/NO ratio (4.79 and r^2=0.95) for the BL air mass increased when the data on 26 and 29 March were excluded. The air mass on 26 March for BL category is likely to be affected by Tula plume, supported by the somewhat similar NO_2/NO ratio (1.54 and r^2=0.99) to that (2.35 and r^2=0.88) for the TIC and by air mass back trajectory analysis (downwind from TIC). In addition, the origin of the air mass on 29 March for BL seems to be changing from rural to urban. In other words, the air mass from about 12:00 to 13:00 local standard time (LST) (NO_2/NO ratio of 1.81 and r^2=0.97) originated from the rural air and from about 13:00–14:00 LST (ratio of 4.17 and r^2=0.77) originated from the polluted MCMA air. The concentration level of NO_x (2.3±4.3 ppbv with median of 0.94) in the data group of the RHS was similar to that for TIC.

High levels of NO_x and NO_y within the megacity result from enhanced local emission sources such as combustion. Thus, NO_x can be a measure of anthropogenic impact at the sampling position. In addition, the ratio of NO_x to NO_y can be valuable for understanding the chemical process as an indicator for photochemical age (Carroll et al., 1992), in spite of several limitations including the assumptions of no physicochemical loss (only dilution of NO_y), no chemical transformation from NO_y to NO_x (e.g., thermal decomposition of PAN), constant emission sources, and constant background concentration. In this field study, the NO_x/NO_y ratio varied from 0.17 (FTCO) to 0.54 (BL), depending on air mass category (Fig. 5). The higher ratios (0.38–0.54) for BL, BB, and TIC (Fig. 5a, b, and e, respectively) indicate less aged air than those (0.17–0.18) for FTCO and FTMA (Fig. 5c and d, respectively). The lower ratios for FTCO and FTMA indicated significant photochemical aging, which is supported by higher ozone production efficiencies, as described below.

The NO_x/NO_y ratios during MIRAGE-Mex were significantly higher than those (0.02–0.2) in continental outflow from East Asia during TRACE-P (Koike et al., 2003). However, the higher ratios (0.38–0.54) for BB, TIC, and BL were comparable to those in the near 2 day aged Asian outflow plume measured during the PEACE-A campaign (Takegawa et al., 2004). Our ratios (0.17–0.18) for the FTCO and FTMA were similar to the ratios (0.13–0.15) for marine air during PEM-Tropics B (Maloney et al., 2001).

3.3 Ozone Production Efficiency (OPE)

Photochemical oxidation of NO_x and its oxidation products were intercorrelated with O_3 formation during the daytime. The OPE, which is the number of O_3 molecules produced per molecule of NO_x oxidized (Kleinman et al., 2002 and references therein), was estimated using the linear regression slope between O_3 and oxidized NO_x products (NO_z=NO_y–NO_x). Figure 6 shows the correlation between odd oxygen (O_3+NO_2) and NO_z and the OPEs for the 5 air mass categories in this field campaign ranged from 4.5 (TIC) to 8.5 (FTMA), indicating both photochemically young and reactive air masses. In general, higher efficiencies (5.9–8.5) were observed in FTCO and FTMA, whereas lower OPEs (4.5–4.6) in TIC and BB. The OPEs in this field campaign were significantly lower than those (73–246) observed in the remote marine atmosphere such as the western North Pacific (Davis et al., 1996), but within the OPE ranges for the urban and rural atmosphere (Marion et al., 2001).

4 Summary and conclusions

Previous studies testing the NO-NO_2 cyclic system were conducted in urban and remote areas using observations of O_3 (R1) and/or peroxy radicals (R3–R4). These earlier studies used the concentrations of model-predicted peroxy radicals test the PSS for NO-NO_2 cyclic system and indicated that the peroxy radicals were not sufficient to explain the observed NO_2/NO ratio. In addition, the model-predicted NO_2 levels in previous studies were reported to be somewhat lower than observations. In this study, we analyzed the NO-NO_2 system in different chemical regimes/air masses based on observations of reactive nitrogen species and peroxy radicals measured during the intensive field campaign of MIRAGE-Mex (4 to 29 March 2006). In general, NO_2/NO ratios seem to be near PSS. For this analysis, the air mass was categorized into 5 groups such as BL, FTCO, FTMA, BB, and TIC. The NO_2/NO ratios for each air mass ranged from 2.35 (TIC) to 5.18 (BB) and NO_x/NO_y ratio varied from 0.17 (FTCO) to 0.54 (BL), indicating both relatively photochemically young and reactive air masses (i.e., OPE ranges from 4.5 (TIC) to 8.5 (FTMA)). The potential role of halogen chemistry in NO_2/NO ratio shift (i.e., lowering the PSS parameter, ϕ) can not be excluded according to our simple calculation of conversion of NO to NO_2 by IO in the marine atmosphere (FTMA case).

Acknowledgements. ZHS was financially supported by the Climate Environment System Research Center sponsored by the SRC program of Korea Science and Engineering Foundation. The National Center for Atmospheric Research is operated by the University Corporation for Atmospheric Research under the sponsorship of the National Science Foundation.

References

Allan, B., McFiggans, G., and Plane, J.: Observations of iodine monoxide in the remote marine boundary layer, J. Geophys. Res., 105, 14 363–14 369, 2000.

Bradshaw, J., Davis, D., Crawford, J., Chen, G., Shetter, R., Müller, M., Gregory, G., Sachse, G., Blake, D., Heikes, B., Singh, H., Mastromarino, J., and Sandholm, S.: Photofragmentation two-photon laser-induced fluorescence detection of NO_2 and NO: Comparison of measurements with model results based on airborne observations during PEM-Tropics A, Geophys. Res. Lett., 26(4), 471–474, doi:10.1029/1999GL900015, 1999.

Cantrell, C. A., Edwards, G. D., Stephens, S., Mauldin, L., Kosciuch, E., Zondlo, M., and Eisele, F.: Peroxy radical observations using chemical ionization mass spectrometry during TOPSE, J. Geophys. Res., 108(D6), 8371, doi:10.1029/2002JD002715, 2003.

Cantrell, C. A., Shetter, R. E., Calvert, J. G., Eisele, F. L., Williams, E., Baumann, K., Brune, W. H., Stevens, P. S., and Mather, J. H.: Peroxy radicals from photostationary state deviations and steady state calculations during the Tropospheric OH Photochemistry Experiment at Idaho Hill, Colorado, 1993, J. Geophys. Res., 102(D5), 6369–6378, doi:10.1029/96JD01703, 1997.

Carroll, M. A., Ridley, B. A., Montzka, D. D., Hübler, G., Walega, J. G., Norton, R. B., Huebert, B. J., and Grahek, F. E.: Measurements of nitric oxide and nitrogen dioxide during the Mauna Loa Observatory Photochemistry Experiment, J. Geophys. Res., 97(D10), 10 361–10 374, 1992.

Chameides, W. L. and Davis, D. D.: Iodine: its possible role in tropospheric chemistry, J. Geophys. Res., 85, 7383–7398, 1980.

Crawford, J., Davis, D., Chen, G., Bradshaw, J., Sandholm, S., Gregory, G., Sachse, G., Anderson, B., Collins, J., Blake, D., Singh, H., Heikes, B., Talbot, R., and Rodriguez, J.: Photostationary state analysis of the NO_2-NO system based on airborne observations from the western and central North Pacific, J. Geophys. Res., 101(D1), 2053–2072, doi:10.1029/95JD02201, 1996.

Crounse, J. D., McKinney, K. A., Kwan, A. J., and Wennberg, P. O.: Measurement of gas-phase hydroperoxides by chemical ionization mass spectrometry (CIMS), Anal. Chem., 78, 6726–6732, 2006

Davis, D. D., Crawford, J., Chen, G., Chameides, W., Liu, S., Bradshaw, J., Sandholm, S., Sachse, G., Gregory, G., Anderson, B., Barrick, J., Bachmeier, A., Collins, J., Browell, E., Blake, D., Rowland, S., Kondo, Y., Singh, H., Talbot, R., Heikes, B., Merrill, J., Rodriguez, J., and Newell, R. E.: Assessment of ozone photochemistry in the western North Pacific as inferred from PEM-West A observations during the fall 1991, J. Geophys. Res., 101(D1), 2111–2134, doi:10.1029/95JD02755, 1996.

Davis, D., Crawford, J., Liu, S., McKeen, S., Bandy, A., Thornton, D., Rowland, F., and Blake, D.: Potential impact of iodine on tropospheric levels of ozone and other critical oxidants, J. Geophys. Res., 101(D1), 2135–2147, doi:10.1029/95JD02727, 1996.

Gregory, G. L., Fuelberg, H. E., Longmore, S. P., Anderson, B. E., Collins, J. E., and Blake, D. R.: Chemical characteristics of tropospheric air over the tropical South Atlantic Ocean: Relationship to trajectory history, J. Geophys. Res., 101(D19), 23 957–23 972, doi:10.1029/96JD01160, 1996.

Kanaya, Y., Tanimoto, H., Matsumoto, J., Furutani, H., Hashimoto, S., Komazaki, Y., Tanaka, S., Yokouchi, Y., Kato, S., Kajii, Y., and Akimoto, H.: Diurnal variations in H_2O_2, O_3, PAN, HNO_3 and aldehyde concentrations and NO/NO_2 ratios at Rishiri Island, Japan: Potential influence from iodine chemistry, Sci. Total Environ., 376, 185–197, 2007.

Kanaya, Y., Yokouchi, Y., Matsumoto, J., Nakamura, K., Kato, S., Tanimoto, H., Furutani, H., Toyota, K., and Akimoto, H.: Implications of iodine chemistry for daytime HO_2 levels at Rishiri Island, Geophys. Res. Lett., 29, 1212, doi.:10.1029/2001GL014061, 2002.

Kleinman, L. I., Daum, P. H., Lee, Y. -N., Nunnermacker, L. J., Springston, S. R., Weinstein-Lloyd, J., and Rudolph, J.: Ozone production efficiency in an urban area, J. Geophys. Res., 107(D23), 4733, doi:http://dx.doi.org/10.1029/ 2002JD002529, 2002.

Knight, G. P. and Crowley, J. N.: The reactions of IO with HO_2, NO and CH_3SCH_3: flow tube studies of kinetics and product formation, Phys. Chem. Chem. Phys., 3, 393–401, 2001.

Koike M., Kondo, Y., Kita, K., et al.: Export of anthropogenic reactive nitrogen and sulfur compounds from the East Asia region in spring, J. Geophys. Res., 108(D20), 8789, doi:10.1029/2002JD003284, 2003.

Li, Q., Jacob, D. J., Bey, I., Yantosca, Y. M., Zhao, Y., Kondo, Y., and Notholt, J.: Atmospheric hydrogen cyanide (HCN): biomass burning source, ocean sink?, Geophys. Res. Lett., 27, 357–360, 2000.

Maloney, J. C., Fuelberg, H. E., Avery, M. A., Crawford, J. H., Blake, D. R., Heikes, B. G., Sachse, G. W., Sandholm, S. T., Singh, H., and Talbot, R. W.: Chemical characteristics of air from different source regions during the second Pacific Exploratory Mission in the Tropics (PEM-Tropics B), J. Geophys. Res., 106(D23), 32 609–32 626, doi:10.1029/2001JD900100,

2001.
Marion, T., Perros, P. E., Losno, R., and Stenier, E.: Ozone production efficiency in Savanna and forested areas during the EXPRESSO experiment, J. Atmos. Chem., 38, 3–30, 2001.
McFiggans, G., Plane, J., Allan, B., and Carpenter, L.: A modeling study of iodine chemistry in the marine boundary layer, J. Geophys. Res., 105(D11), 14 371–14 385, 2000.
Nunnermacker, L. J., Kleinman, L. I., Imre, D., Daum, P. H., Lee, Y.-N., Lee, J. H., Springston, S. R., Newman, L., and Gillani, N.: NO_y lifetimes and O_3 production efficiencies in urban and power plant plumes: Analysis of field data, J. Geophys. Res., 105(D7), 9165–9176, doi:10.1029/1999JD900753, 2000.
Raga, G. and Raga, A.: On the formation of an elevated ozone peak in Mexico City, Atmos. Environ., 34, 4097–4102, 2000.
Raga, G., Baumgardner, D., Castro, T., Martínez-Arroyo, A., and Navarro-González, R.: Mexico City air quality: a qualitative review of gas and aerosol measurements (1960–2000), Atmos. Environ., 35, 4041–4058, 2001.
Ridley, B. A., Madronich, S., Chatfield, R. B., Walega, J. G., Shetter, R. E., Carroll, M. A., and Montzka, D. D.: Measurements and model simulations of the photostationary state during MLOPEX: Implications for radical concentrations and ozone production and loss rates, J. Geophys. Res., 97, 10 375–10 388, 1992.
Saiz-Lopez, A. and Plane, J. M. C.: Novel iodine chemistry in the marine boundary layer, Geophys. Res. Lett., 31, L04112, doi:10.1029/2003GL019215, 2004.
Sander, S. P., Friedl, R. R., Golden, D. M., Kurylo, M. J., Moortgat, G. K., Ravishankara, A. R., Kolb, C. E., Molina, M. J., and Finlayson-Pitts, B. J.: Chemical kinetics and photochemical data for use in stratospheric modeling, Jet Propulsion Laboratory Publication 02–25, Jet Propulsion Laboratory, Pasadena, California, 2002.
Shetter, R. E., Cinquini, L., Lefer, B. L., Hall, S. R., and Madronich, S.: Comparison of airborne measured and calculated spectral actinic flux and derived photolysis frequencies during the PEM Tropics B mission, J. Geophys. Res., 107, 8234, doi:10.1029/2001JD001320, 2002, (printed 108 (D2), 2003).
Slusher D. L., Huey, L. G., Tanner, D. J., Flocke, F. M., and Roberts. J. M.: A thermal dissociation–chemical ionization mass spectrometry (TD-CIMS) technique for the simultaneous measurement of peroxyacyl nitrates and dinitrogen pentoxide, J. Geophys. Res., 109, D19315, doi:10.1029/2004JD004670, 2004.
Soltic, P. and Weilenmann, M.: NO_2/NO emissions of gasoline passenger cars and light-duty

trucks with Euro-2 emission standard, Atmos. Environ., 37, 5207–5216, 2003.

Takegawa, N., Kondo, Y., Koike, M., et al.: Removal of NO_x and NO_y in Asian outflow plumes: Aircraft measurements over the western Pacific in January 2002, J. Geophys. Res., 109, D23S04, doi:10.1029/2004JD004866, 2004.

Tie, X., Madronich, S., Li, G. H., Ying, Z., Zhang, R., Garcia, A. R., Lee-Taylor, J., and Liu, Y.: Characterizations of chemical oxidants in Mexico City: A regional chemical dynamical model (WRF-Chem) study, Atmos. Environ., 41, 1989–2008, 2007.

Weinheimer, A. J., Montzka, D. D., Campos, T. L., et al.: Comparison between DC-8 and ER-2 species measurements in the tropical middle troposphere: NO, NO_y, O_3, CO_2, CH_4, and N_2O, J. Geophys. Res., 103(D17), 22 087–22 096, 1998.

Yokelson, R., Urbanski, S., Atlas, E., Toohey, D., Alvarado, E., Crounse, J., Wennberg, P., Fisher, M., Wold, C., Campos, T., Adachi, K., Buseck, P. R., and Hao, W. M.: Emissions from forest fires near Mexico City, Atmos. Chem. Phys. Discuss., 7, 6687–6718, 2007, http://www.atmos-chem-phys-discuss.net/7/6687/2007/.

Table 1. Temporal and spatial information on airborne sample acquisition during the studyperiod.

Flight No.	Date	Time (LST)	Altitude (km)	Latitude (° N)	Longitude (° W)
1	04-March-06	11:56–19:21	0.02–5.81	17°35′–19°38′	97°52′–103°54′
2	08-March-06	11:06–17:52	0.02–5.36	16° 37′–19° 46′	97° 50′–102° 14′
3	10-March-06	09:20–17:26	0.02–8.12	19° 00′–21° 58′	94° 04′–100° 35′
4	12-March-06	11:02-19:09	0.02-5.80	18° 17′–23° 23′	96° 10′–100° 58′
5	16-March-06	09:20–18:07	0.03–5.63	17°57′–21°32′	97°49′–103°49′
6	18-March-06	08:47–17:18	0.03–5.69	19°00′-22°17′	97°50′-101°22′
7	19-March-06	11:03–19:47	0.02–5.64	18°59′–27°22′	93°09′–100°36′
8	22-March-06	09:17–16:15	0.03–5.20	19°06′–21°11′	96°42′–100°33′
9	23-March-06	10:53–16:59	0.03–5.62	18°06′–21°06′	89°19′–98°38′
10	26-March-06	10:56–13:13	0.03–5.39	18°59′–20°15′	97°50′–100°43′
11	28-March-06	03:44–11:07	0.03–6.70	19°04′–22°03′	96°45′–99°04′
12	29-March-06	10:39–17:26	0.03–6.77	18°35′–20°06′	95°27′–100°23′

ACPD
8, 2275–2309, 2008

Table 2. A statistical summary of reactive nitrogen compounds, major air pollutants, and peroxy radicals with air mass categories measured during the MIRAGE fieldcampaign.

Air mass category*	NO (ppbv)	NO_2 (ppbv)	NO_x (ppbv)	NO_y (ppbv)	CO (ppbv)	O_3 (ppbv)	SO_2 (ppbv)	HO_2 (pptv)	RO_2 (pptv)
BL	0.7±1.1[a] 0.27[b] 0.01–7.8[c] 387[d]	3.0±4.2 1.0 0.07–27 387	3.7±5.1 1.3 0.09–32 387	7.8±7.4 4.9 0.9–37 375	249±110 223 111–688 170	79±25 76 32–153 396	4.7±17.9 1.9 0.2–207 278	77±49 55 12–246 267	54±48 35 0.8–241 255
BB	0.5±0.8 0.2 0.02–4.0 88	2.5±4.6 0.7 0.06–23 88	3.1±5.3 0.9 0.08–26 88	10.2±11.5 6.3 0.7–59 86	278±184 225 81–937 58	74±30 72 29–151 90	2.7±2.1 2.0 0.2–9.7 60	58±26 59 12–106 24	159±71 158 58–362 30
FTCO	0.05±0.09 0.03 0–1.7 1125	0.2±0.4 0.1 0.01–5.7 1185	0.3±0.5 0.2 0.03–7.4 1132	1.7±2.6 1.3 0.06–25 1057	128±41 119 69–424 636	51±14 50 0.4–144 1246	2.0±6.8 0.68 0–120 687	45±33 40 0.01–353 778	43±38 29 0.02–194 564
FTMA	0.06±0.1 0.03 0–1.9 561	0.3±0.4 0.1 0.02–4.2 563	0.3±0.6 0.1 0.03–4.9 561	2.0±2.2 1.4 0.1–16 519	123±64 112 60–416 351	57±17 57 29-129 595	1.4±1.6 0.93 0–10.0 375	30±20 29 0.1–129 237	22±17 21 0.3–190 206
TIC	0.7±1.3 0.2 0.02–7.4 69	2.0±3.1 0.6 0.03–19 69	2.6±4.4 0.8 0.05–26 69	8.5±7.4 6.0 0.3–40 67	186±81 192 67–418 59	72±19 74 40–120 70	22.3±40.4 9.4 0.15–235 43	12±4 13 8–18 5	101±42 108 10–168 30

[a] Mean±1σ; [b] Median; [c] Min.–Max.; [d] Number of data. * The category for the BL air masses was determined based on meteorological parameters and WRF-Chem; those for FTCO and FTMA based on geographical locations of airborne sampling; that for the BB based on hydrogen cyanide (HCN), perchlorethene (C_2Cl_4), and CO; and that for TIC based on the concentration levels of CO, NO_x, and SO_2.

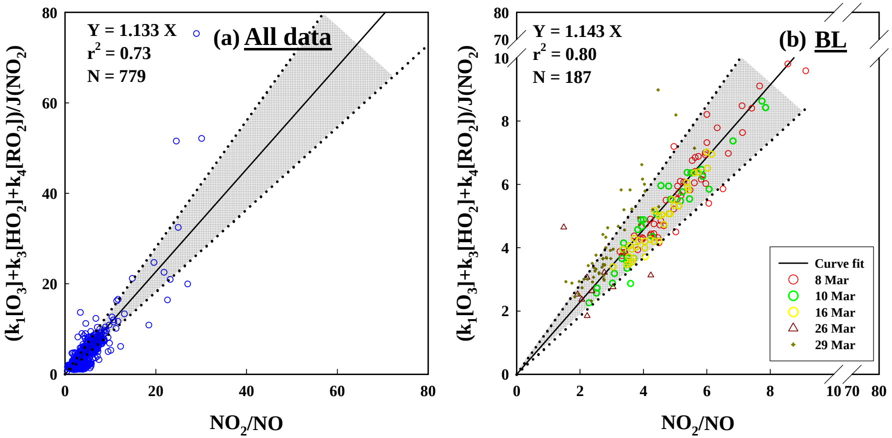

Fig. 1. Photostationary state analysis for the NO-NO_2 system during the MIRAGE-Mex field campaign (4 March to 29 March 2006) for 5 air mass categories (all **(a)**, BL **(b)**, BB **(c)**, FTCO **(d)**, FTMA **(e)**, and TIC **(f)**). The photostationary parameter ϕ is the slope of these plots. The uncertainty ranges (1σ) of ϕ for the 5 air mass categories (23–25%) are denoted by grey shading.

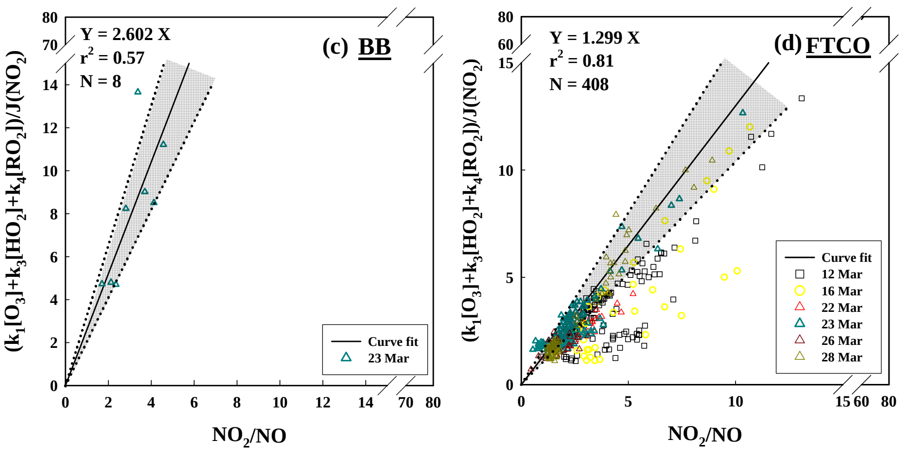

Fig. 1. Continued.

ACPD
8, 2275–2309, 2008

Characteristics of the $NO-NO_2-O_3$ system during the MIRAGE-Mex

Z.-H. Shon et al.

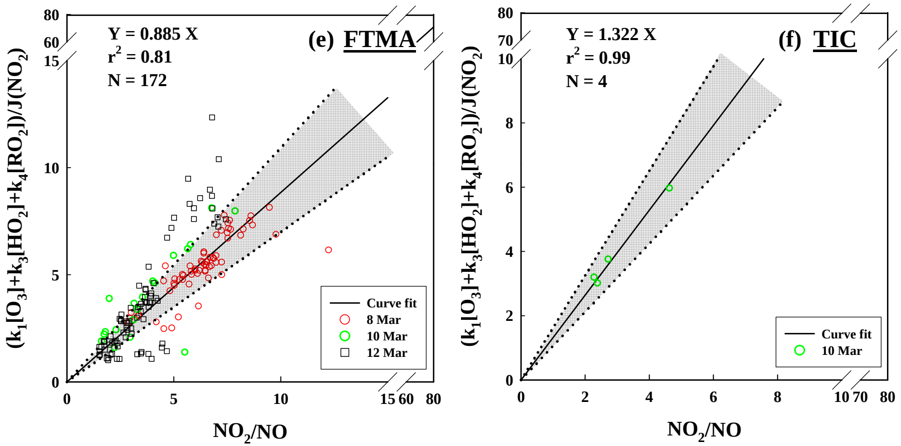

Fig. 1. Continued.

ACPD

8, 2275–2309, 2008

Title Page
Abstract | Introduction
Conclusions | References
Tables | Figures
◀| |▶
◀ ▶
Back | Close
Full Screen / Esc
Printer-friendly Version
Interactive Discussion

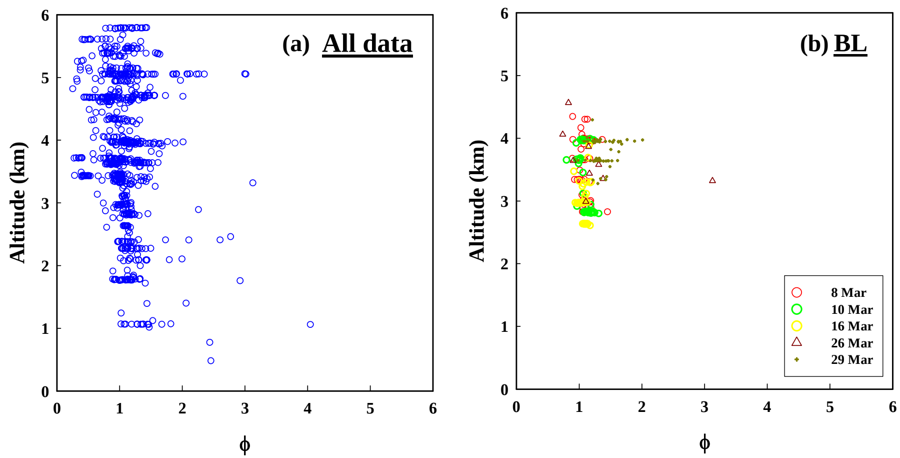

Fig. 2. Vertical profile of the PSS parameter (ϕ) for 5 air mass categories (all **(a)**, BL **(b)**, BB **(c)**, FTCO **(d)**, FTMA **(e)**, and TIC **(f)**).

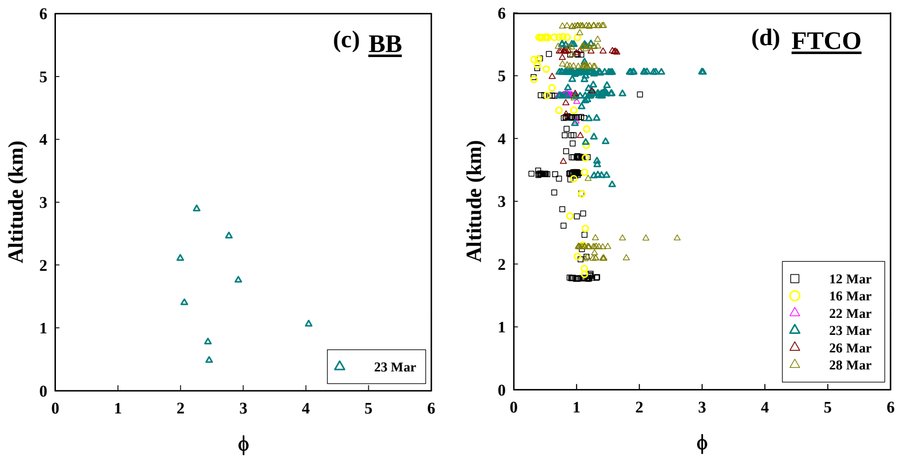

Fig. 2. Continued.

ACPD
8, 2275–2309, 2008

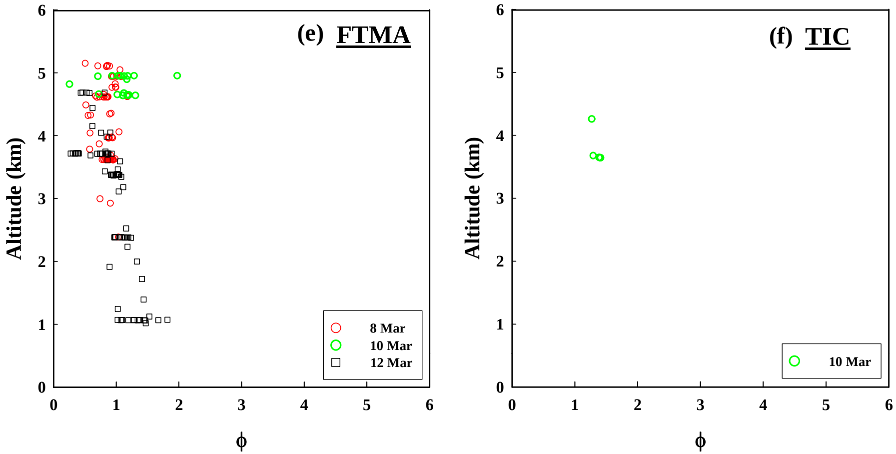

Fig. 2. Continued.

ACPD
8, 2275–2309, 2008

Characteristics of the $NO-NO_2-O_3$ system during the MIRAGE-Mex

Z.-H. Shon et al.

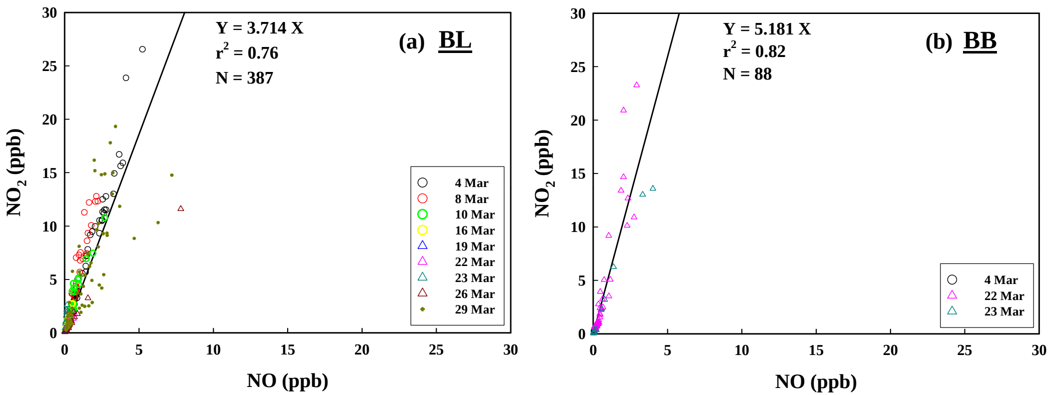

Fig. 3. Correlation between NO and NO_2 for 5 air mass categories (BL **(a)**, BB **(b)**, FTCO **(c)**, FTMA **(d)**, and TIC **(e)**).

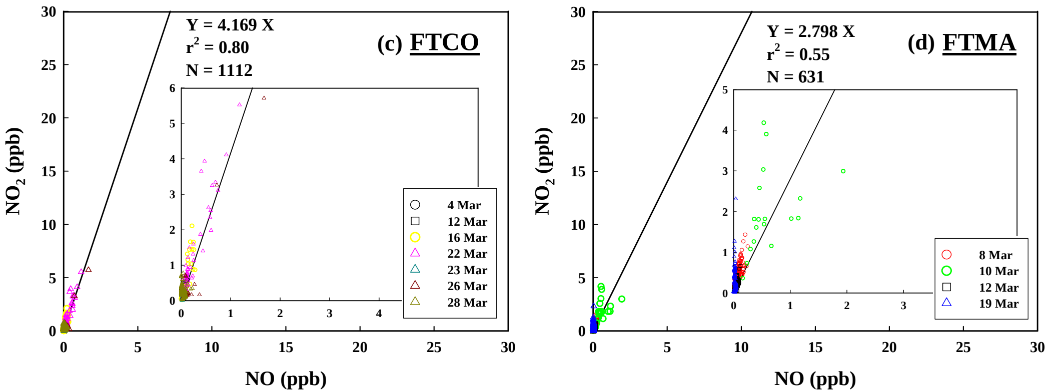

Fig. 3. Continued.

ACPD
8, 2275–2309, 2008

Characteristics of the NO-NO_2-O_3 system during the MIRAGE-Mex

Z.-H. Shon et al.

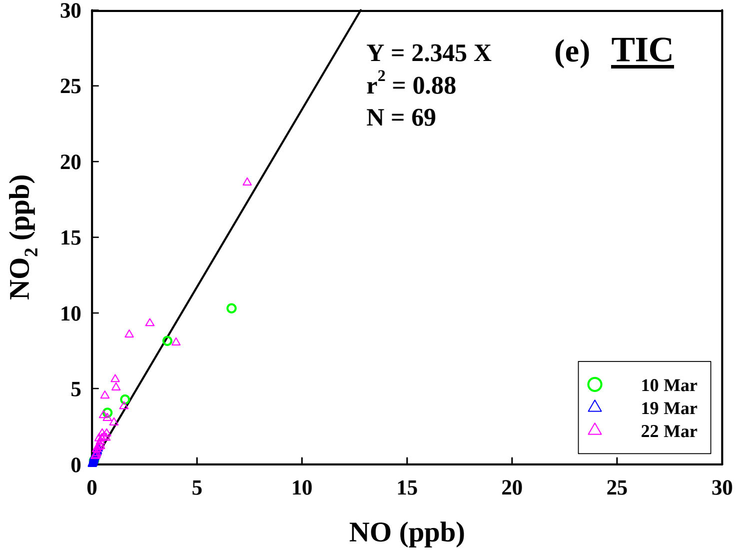

Fig. 3. Continued.

ACPD
8, 2275–2309, 2008

Title Page
Abstract Introduction
Conclusions References
Tables Figures
◂ ▸
Back Close
Full Screen / Esc
Printer-friendly Version
Interactive Discussion

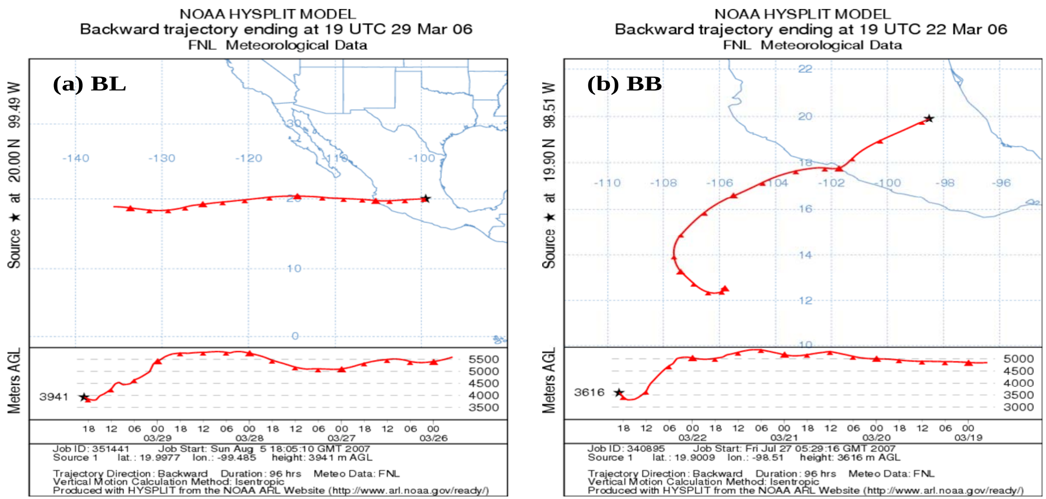

Fig. 4. Air mass back trajectory analysis for 5 air mass categories (BL **(a)**, BB **(b)**, FTCO **(ac**, FTMA **(d)**, and TIC **(e)**), which are the most frequent air mass back trajectory for each air mass category.

ACPD

8, 2275–2309, 2008

Title Page
Abstract | Introduction
Conclusions | References
Tables | Figures
◀| |▶
◀ ▶
Back | Close
Full Screen / Esc
Printer-friendly Version
Interactive Discussion

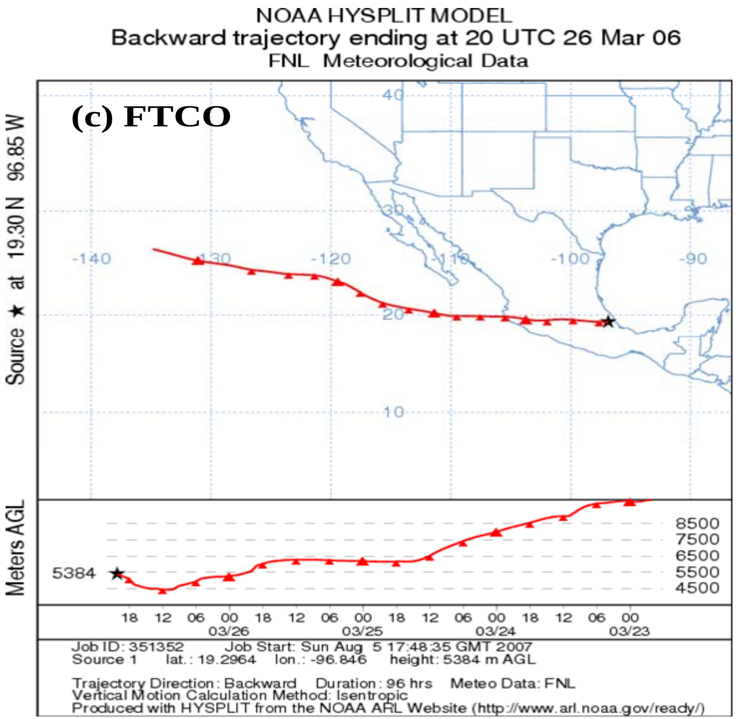

Fig. 4. Continued.

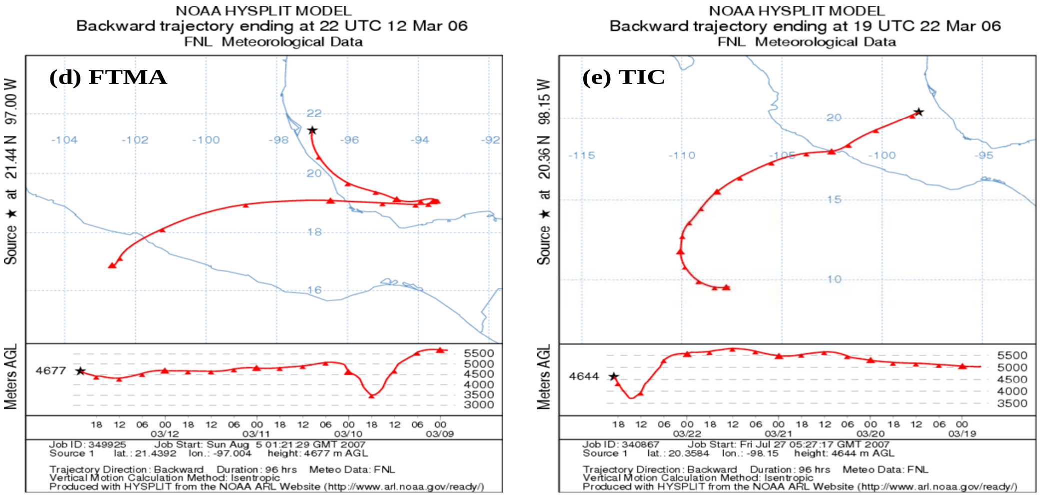

Fig. 4. Continued.

ACPD
8, 2275–2309, 2008

Z.-H. Shon et al.

ACPD

8, 2275–2309, 2008

Characteristics of the $NO\text{-}NO_2\text{-}O_3$ system during the MIRAGE-Mex

Z.-H. Shon et al.

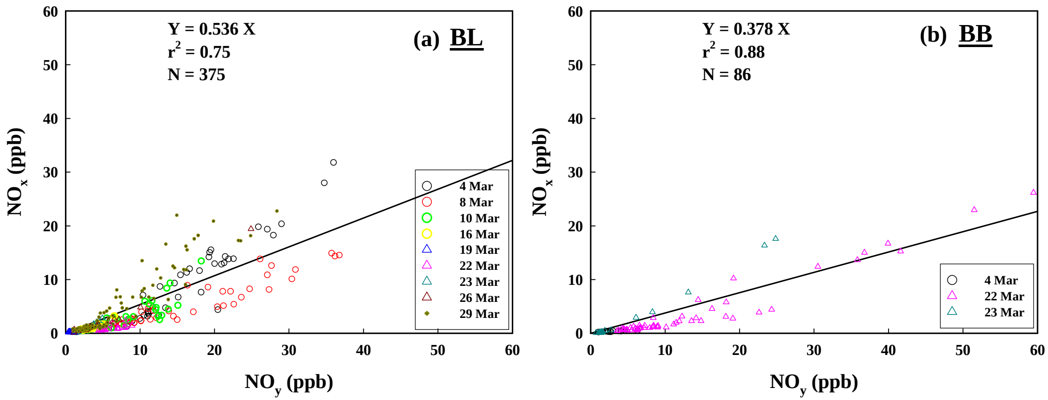

Fig. 5. Correlation between NO_x and NO_y for 5 air mass categories (BL **(a)**, BB **(b)**, FTCO **(c)**, FTMA **(d)**, and TIC **(e)**).

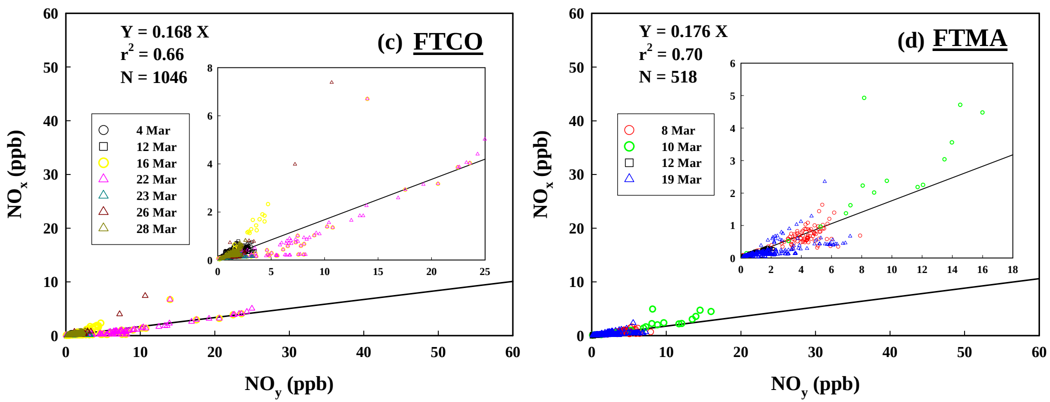

Fig. 5. Continued.

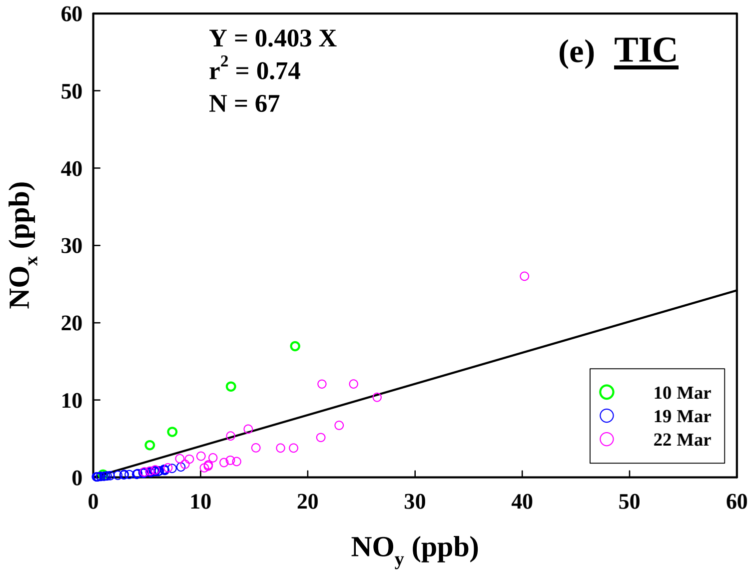

Fig. 5. Continued.

ACPD
8, 2275–2309, 2008
Characteristics of the NO-NO_2-O_3 system during the MIRAGE-Mex
Z.-H. Shon et al.

ACPD

8, 2275–2309, 2008

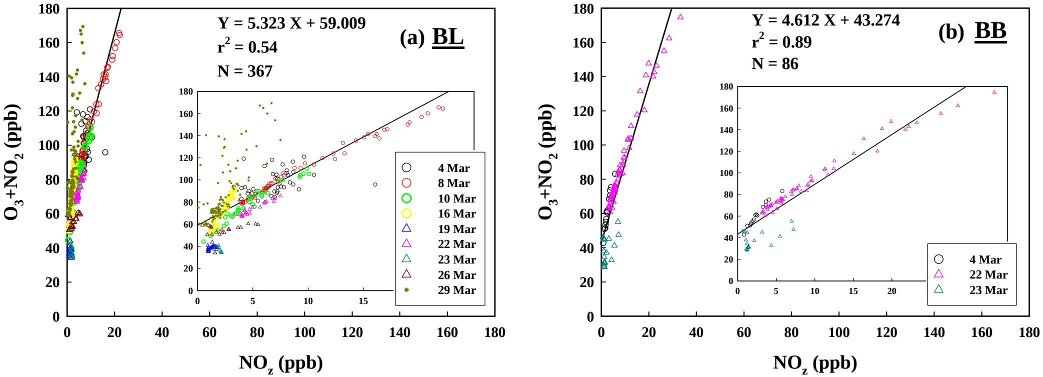

Fig. 6. Correlation between O_3+NO_2 and NO_z for 5 air mass categories (BL **(a)**, BB **(b)**, FTCO **(c)**, FTMA **(d)**, and TIC **(e)**).

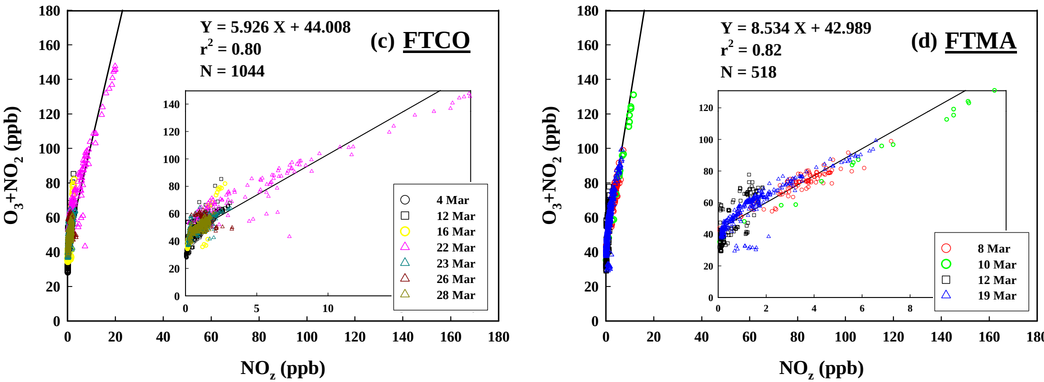

Fig. 6. Continued.

ACPD
8, 2275–2309, 2008

Characteristics of the $NO-NO_2-O_3$ system during the MIRAGE-Mex

Z.-H. Shon et al.

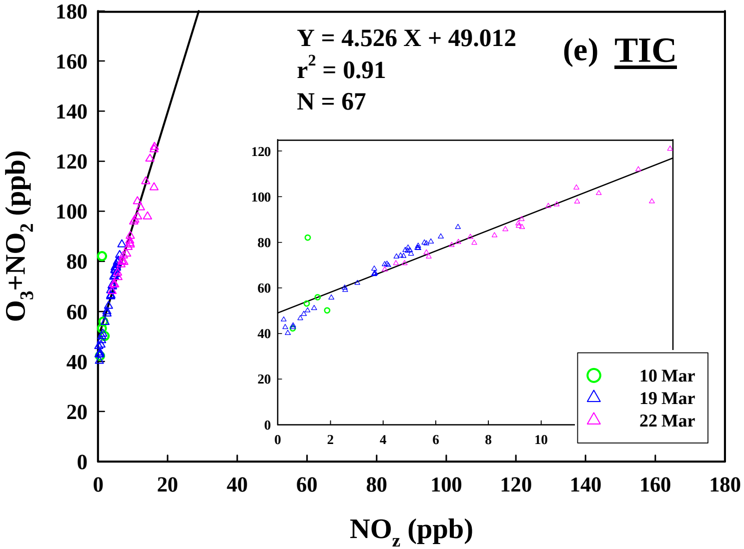

Fig. 6. Continued.

ACPD
8, 2275–2309, 2008

Characteristics of the $NO-NO_2-O_3$ system during the MIRAGE-Mex

Z.-H. Shon et al.